

Tunable isolated attosecond X-ray pulses with gigawatt peak power from a free-electron laser

Joseph Duris^{1,12}, Siqi Li^{1,2,12}, Taran Driver^{1,3,4}, Elio G. Champenois³, James P. MacArthur^{1,2}, Alberto A. Lutman¹, Zhen Zhang¹, Philipp Rosenberger^{1,3,5,6}, Jeff W. Aldrich¹, Ryan Coffee¹, Giacomo Coslovich¹, Franz-Josef Decker¹, James M. Glowia¹, Gregor Hartmann⁷, Wolfram Helml^{1,6,8,9}, Andrei Kamalov^{2,3}, Jonas Knurr³, Jacek Krzywinski¹, Ming-Fu Lin¹, Jon P. Marangos^{1,4}, Megan Nantel^{1,2}, Adi Natan^{1,3}, Jordan T. O'Neal^{2,3}, Niranjan Shivaram¹, Peter Walter¹, Anna Li Wang^{3,10}, James J. Welch¹, Thomas J. A. Wolf³, Joseph Z. Xu¹¹, Matthias F. Kling^{1,3,5,6}, Philip H. Bucksbaum^{1,2,3,10}, Alexander Zholents¹¹, Zhirong Huang^{1,10}, James P. Cryan^{1,3*} and Agostino Marinelli^{1*}

The quantum-mechanical motion of electrons in molecules and solids occurs on the sub-femtosecond timescale. Consequently, the study of ultrafast electronic phenomena requires the generation of laser pulses shorter than 1 fs and of sufficient intensity to interact with their target with high probability. Probing these dynamics with atomic-site specificity requires the extension of sub-femtosecond pulses to the soft X-ray spectral region. Here, we report the generation of isolated soft X-ray attosecond pulses with an X-ray free-electron laser. Our source has a pulse energy that is millions of times larger than any other source of isolated attosecond pulses in the soft X-ray spectral region, with a peak power exceeding 100 GW. This unique combination of high intensity, high photon energy and short pulse duration enables the investigation of electron dynamics with X-ray nonlinear spectroscopy and single-particle imaging, unlocking a path towards a new era of attosecond science.

The natural timescale of electron motion in molecular systems is determined by the binding energy, I_p , typically between 8 and 12 eV. Quantum mechanics tells us that this relationship is given by $\tau = \hbar/I_p$, where \hbar is the reduced Planck constant. Therefore, the relevant timescale for electron motion in molecular systems is on the order of a few hundred attoseconds (1 as = 10^{-18} s). Isolated light pulses approaching this extreme timescale were first demonstrated in 2001¹. These early demonstrations employed a process called high-harmonic generation (HHG), where a strong, infrared laser field was used to coherently drive electrons in an atomic or molecular gas, leading to high-order harmonic upconversion of the driving laser field². The extension of time-resolved spectroscopy into the attosecond domain has greatly advanced our understanding of electron dynamics in atoms, molecules and condensed-matter systems^{3–5}. This attosecond revolution has been almost exclusively driven by HHG-based sources^{1,6–17}, which have been recently extended to reach soft X-ray wavelengths (above 280 eV) and produce the shortest pulses ever recorded^{18–21}. Extending attosecond pulse sources into the soft X-ray domain is particularly important because soft X-rays can access core-level electrons whose absorption properties are sensitive probes of transient electronic structure^{22–24}. Despite these recent achievements in soft X-ray HHG, the wavelength scaling of the HHG process leads to a rapid decrease in conversion efficiency with increasing X-ray photon energy²⁵. This presents a real challenge for the progress of attosecond

science. For example, the current paradigm based on long-wavelength high-power lasers is limiting our exploration of coherent electronic phenomena in complex systems because of the non-perturbative nature of strong-field interactions. This could be circumvented with soft X-ray attosecond pump/attosecond probe techniques^{26,27} that require intense X-ray pulses.

In parallel with the development of HHG, the last two decades have seen the rise of X-ray free-electron lasers (XFELs), such as the Linac Coherent Light Source (LCLS), as the brightest sources of X-ray radiation^{28–34}. The working principle of an XFEL is based on the interaction of a relativistic electron beam with an X-ray electric field in a long periodic array of magnetic dipoles called an undulator^{35–37}. The radiation–electron interaction causes the electron beam to reorganize itself in a sequence of microbunches shorter than the radiation wavelength, which results in the coherent emission of X-ray radiation with a peak power many orders of magnitude larger than the spontaneous level^{36,37}. Compared with laser-based HHG sources, XFELs have a large extraction efficiency at X-ray wavelengths—typically of order of 0.1% or larger. With a typical electron beam peak power in the tens of terawatts range, the resulting X-ray pulses have tens of gigawatts of peak power, several orders of magnitude larger than table-top X-ray sources. Furthermore, the photon energy of XFEL sources is easily tunable via small configuration changes of the accelerator or the undulator. The shortest pulse achievable with an XFEL is limited by the available amplification

¹SLAC National Accelerator Laboratory, Menlo Park, CA, USA. ²Physics Department, Stanford University, Stanford, CA, USA. ³Stanford PULSE Institute, SLAC National Accelerator Laboratory, Menlo Park, CA, USA. ⁴The Blackett Laboratory, Imperial College London, London, UK. ⁵Max Planck Institute of Quantum Optics, Garching, Germany. ⁶Physics Department, Ludwig-Maximilians-Universität Munich, Garching, Germany. ⁷Institut für Physik und CINSaT, Universität Kassel, Kassel, Germany. ⁸Zentrum für Synchrotronstrahlung, Technische Universität Dortmund, Dortmund, Germany. ⁹Physik-Department E11, Technische Universität München, Garching, Germany. ¹⁰Applied Physics Department, Stanford University, Stanford, CA, USA. ¹¹Argonne National Laboratory, Lemont, IL, USA. ¹²These authors contributed equally: Joseph Duris, Siqi Li. *e-mail: jcryan@slac.stanford.edu; marinelli@slac.stanford.edu

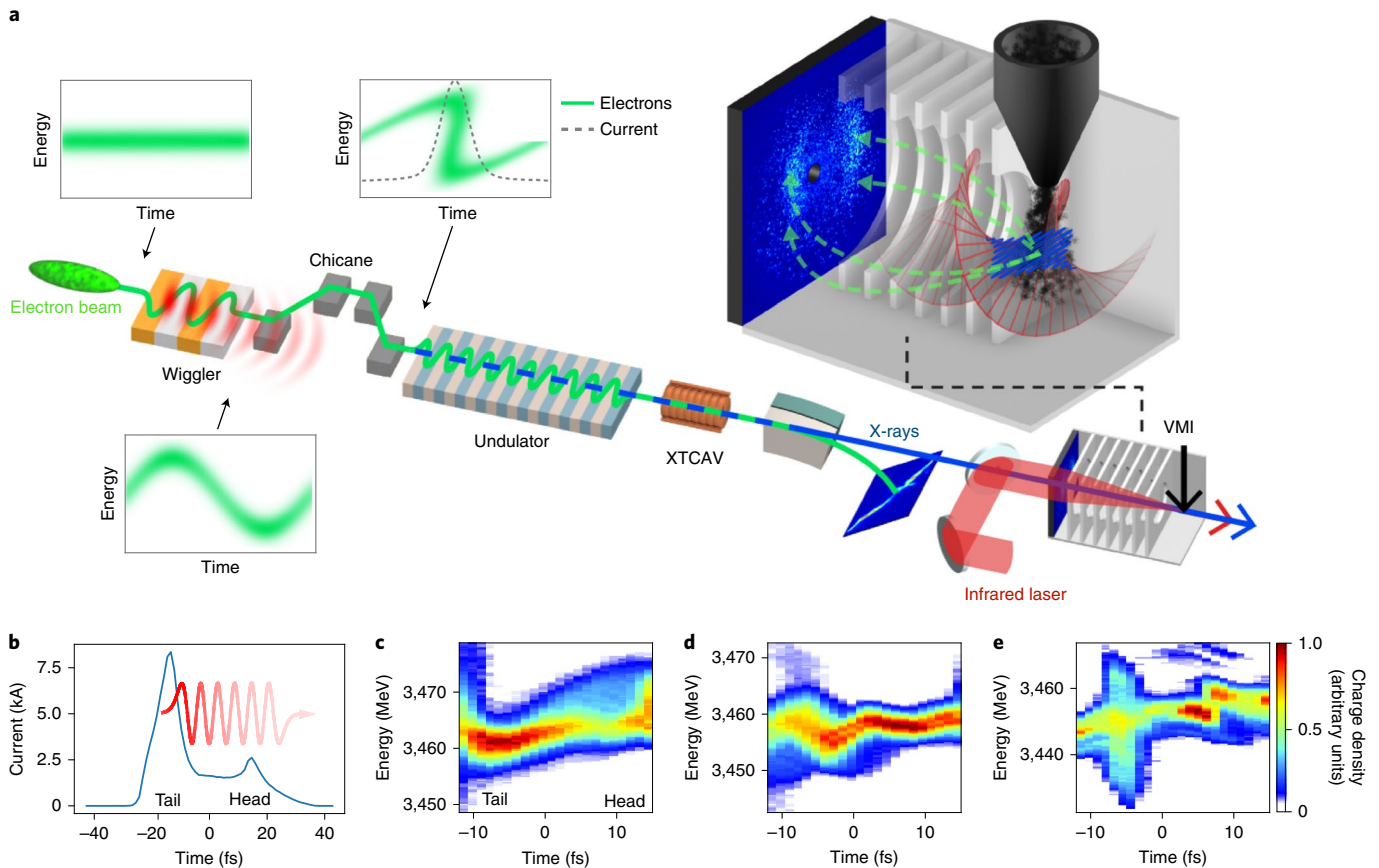


Fig. 1 | Diagram of the XLEAP operation. **a**, Schematic representation of the experiment. The electron beam travels through a long-period (35 cm) wiggler and develops a single-cycle energy modulation. The energy modulation is turned into a density spike by a magnetic chicane and sent to the LCLS undulator to generate sub-femtosecond X-ray pulses. After the undulator, the relativistic electrons are separated from the X-rays and sent to a transverse cavity (labelled XTCAV) used for longitudinal measurements of the beam. The X-rays are overlapped with a circularly polarized infrared laser and interact with a gas jet to generate photoelectrons. The ejected photoelectrons are streaked by the laser and detected with a velocity map imaging (VMI) spectrometer. The momentum distribution of the electrons is used to reconstruct the pulse profile in the time domain. **b–e**, The measurements of the ESASE modulation process. **b**, The measured current profile of the electron bunch generated by the accelerator. The tail of the bunch has a high-current horn that generates a high-power infrared pulse, represented by the red squiggle, which is used for the ESASE compression. **c–e**, The longitudinal phase space of the core of the electron bunch in three different conditions: with no wiggler and no chicane we measure the electron distribution generated by the accelerator (**c**); after inserting the wiggler we observe a single-cycle energy modulation generated by the interaction between electrons and radiation (**d**); after turning on the chicane the modulation is turned into a high-current spike at $t = -5$ fs (**e**).

bandwidth, which is of similar magnitude to their extraction efficiency $\sim 0.1\%$ ^{35,38}. For example, the X-ray bandwidth of the LCLS can support pulses shorter than 1 fs for hard X-ray energies^{39,40}. However, the shortest possible pulse duration increases to 1–2 fs for photon energies below 1 keV (refs. ^{41,42}), where the relevant core-level absorption edges for light elements are found: carbon (280 eV), nitrogen (410 eV) and oxygen (540 eV). Here we report the generation and time-resolved measurement of hundred-gigawatt-scale isolated attosecond soft X-ray pulses with an XFEL. The bandwidth limitation of the XFEL was overcome by compressing the electron beam through the resonant interaction of the electrons with a high-power infrared pulse generated by the beam itself.

Figure 1a shows a schematic representation of our experimental set-up, named X-ray laser-enhanced attosecond pulse generation (XLEAP). The energy distribution of the electron beam is modulated by the resonant interaction with a high-power infrared laser pulse in a long-period undulator (or wiggler). This modulation is converted into one or more high-current (~ 10 kA) spikes by a magnetic chicane. The spikes are subsequently used in the undulator to generate short X-ray pulses, a method termed enhanced self-amplified spontaneous emission (ESASE)⁴³. This bunch

compression method effectively broadens the XFEL bandwidth and allows the generation of sub-femtosecond pulses in the soft X-ray spectral region. In our experiment, rather than using an external infrared laser as originally proposed by Zholtens⁴³, we employ the coherent infrared radiation emitted by the tail of the electron beam in the wiggler to modulate the core of the electron beam⁴⁴. This method results in a phase-stable, quasi-single-cycle modulation, and naturally produces a single high-current spike that can generate an isolated attosecond pulse. Figure 1b–e shows the measured initial current profile and the evolution of the phase space of the core of the electron bunch during the three stages of ESASE compression.

After separating the broad bandwidth X-ray pulses from the spent electron bunch, the X-ray pulses are focused and temporally overlapped with a circularly polarized, 1.3 μm , infrared laser field in a velocity map imaging spectrometer⁴⁵. Photoelectrons ionized by the X-ray pulse receive a ‘kick’ proportional to the vector potential of the infrared laser pulse at the time of ionization⁴⁶. Through the interaction of the ionized electron with the dressing infrared laser field, the temporal properties of the X-ray pulse are mapped onto the final momentum distribution of the emitted photoelectrons^{47–49}. This technique was originally called the ‘attosecond streak camera’,

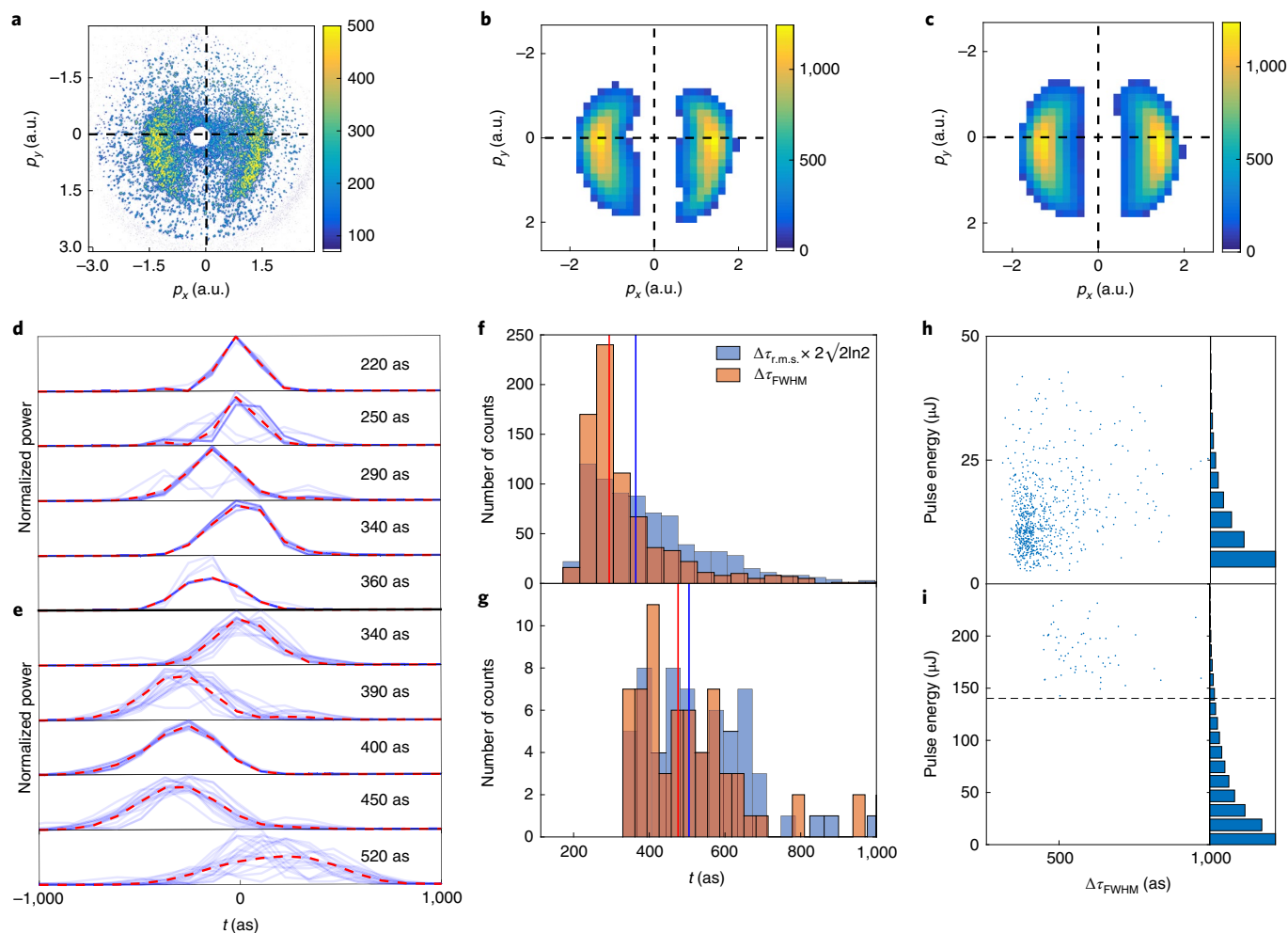


Fig. 2 | Results of the angular streaking measurement. a–c, Measured and reconstructed streaked photoelectron distribution from a single X-ray pulse. Our reconstruction algorithm reads the photoelectron momentum distribution (**a**), downsamples the data (**b**) and fits them to simulated streaked spectra calculated from a complete basis set (**c**). In this single-shot example the infrared laser vector potential was directed roughly in the negative p_y direction at the time of arrival of the X-ray pulse. a.u., atomic units. **d,e,** Representative pulse reconstruction at 905 eV (**d**) and 570 eV (**e**). The shaded blue lines are the solutions found from running the reconstruction algorithm initiated by different random seeds, and the red lines are the most probable solution (see Supplementary Information for details). The labelled number is the averaged $\Delta\tau_{\text{FWHM}}$ over the different solutions. **f,g,** Distribution of retrieved X-ray pulse durations for 905 eV (**f**) and 570 eV (**g**). The red and blue vertical lines correspond to the median of $\Delta\tau_{\text{FWHM}}$ and $\Delta\tau_{\text{r.m.s.}} \times 2\sqrt{2\ln 2}$, respectively (r.m.s., root mean square). For the 905 eV data, these values are 280 as and 360 as. For the 570 eV data, they are 480 as and 510 as. **h,i,** Scatter plot of pulse energy as a function of pulse duration for the reconstructed shots and a histogram of the pulse energy for the entire dataset for 905 eV (**h**) and 570 eV (**i**). Note that for the 570 eV data the reconstruction fails to converge under 130 μJ (region below the dashed line) due to a different gas density setting and low count rates, but since there is no correlation between pulse duration and pulse energy we believe the data points are representative of the entire dataset.

and is routinely used to measure the temporal profile of isolated attosecond pulses from HHG sources³⁰. In contrast to measurements done with HHG sources, in this work we are able to diagnose the single-shot pulse profile, rather than an average pulse shape. Moreover, the shot-to-shot fluctuations (or jitter) in the relative arrival time between the X-ray and optical field present at an XFEL facility⁵¹ makes single-shot measurements necessary. This measurement scheme was originally demonstrated with X-rays at the LCLS by Hartmann et al., who recovered the ‘time–energy structure’ of self-amplified spontaneous emission (SASE) pulses produced by the LCLS¹². We have adapted this technique to measure the sub-femtosecond structure of the X-ray pulses produced by XLEAP.

Results

Figure 2a shows a single-shot measurement of the ‘streaked’ photoelectron momentum distribution, which we use to reconstruct the full temporal profile of the X-ray pulse⁴⁹. The raw data are filtered

and downsampled (Fig. 2b) before being fed into the reconstruction algorithm, which returns a pulse profile and corresponding photoelectron distribution (Fig. 2c). The robustness of this algorithm has been tested at length in ref. 49, and is detailed in the Supplementary Information. Figure 2 also shows representative temporal profiles retrieved from the reconstruction at photon energies of 905 eV (Fig. 2d) and 570 eV (Fig. 2e). Figures 2f and g show the distribution of pulse widths (full-width at half-maximum (FWHM) of the intensity profile) retrieved from two large datasets at these photon energies. The data show that the XLEAP set-up generates sub-femtosecond X-ray pulses, and we find a median duration of 280 as FWHM (480 as) at 905 eV (570 eV). The pulse duration fluctuates on a shot-to-shot basis and half of the single-shot measurements fall within a 110 as (170 as) window at 905 eV (570 eV). This amount of fluctuation is consistent with numerical simulations of ESASE XFEL operation (see for example ref. 52). The estimated uncertainty on the single-shot pulse duration is between 10% and 30% of the

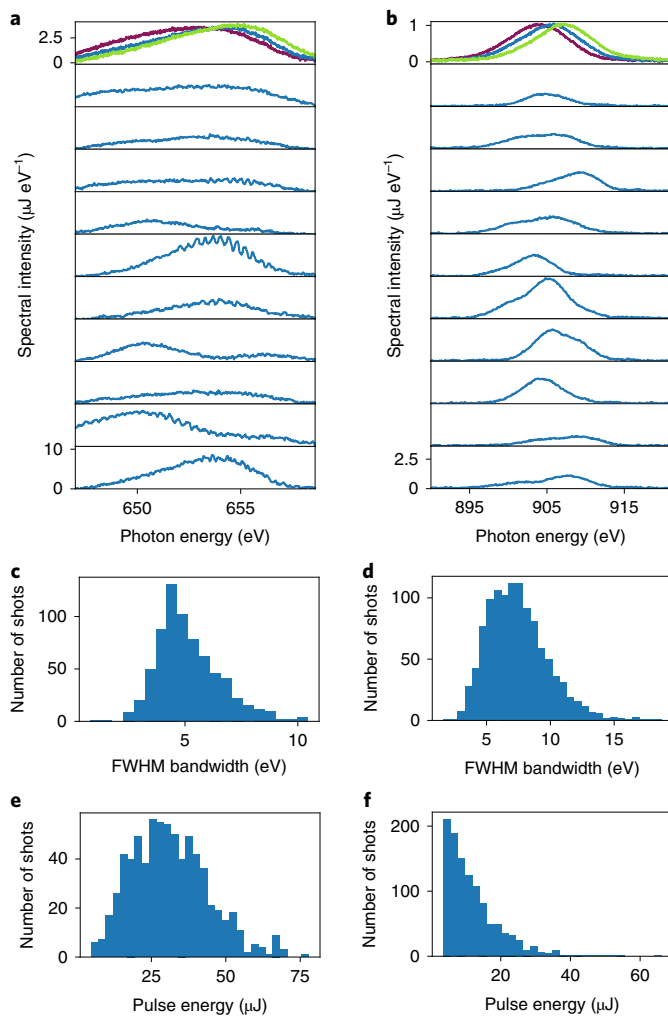


Fig. 3 | Spectral measurements. **a, b**, Spectra of the attosecond X-ray pulses measured with a grating spectrometer at two different electron beam energies (3,782.1 MeV (**a**) and 4,500.3 MeV (**b**)). The upper panels in **a** and **b** show average spectra at slightly different electron beam energies (in steps of 2.7 MeV for 650 eV and 3.0 MeV steps for 905 eV, where green corresponds to the highest energy and purple to the lowest), while the remaining spectra show single-shot measurements at the central beam energy. **c, d**, Histograms of the distribution of FWHM bandwidths. **e, f**, Histograms of the distribution of pulse energies.

measured duration depending on the pulse energy and the amplitude of the streaking laser field (a discussion on the experimental uncertainty of the measurement can be found in the Supplementary Information). The median pulse energy is 10 μJ at 905 eV and 25 μJ at 570 eV. However, due to the intrinsic fluctuations of SASE XFELs³⁸ we observe pulses well above the mean value (up to 250 μJ for 570 eV, corresponding to a peak power in the hundreds of gigawatts). We note that for the 570 eV dataset we were only able to obtain converging reconstructions for pulse energies higher than 130 μJ , corresponding to the top 8%, due to a different gas density setting and lower count rates. However, since the data at both energies do not show a significant correlation between pulse energy and duration (Fig. 2h,i) we believe that the average pulse duration from this sample is representative of the entire dataset.

In a separate set of experiments, we measured single-shot X-ray spectra with a grating spectrometer. Figure 3 shows a range of single-shot X-ray spectra recorded for 650 eV and 905 eV photon energies, and the distribution of the measured bandwidth (FWHM).

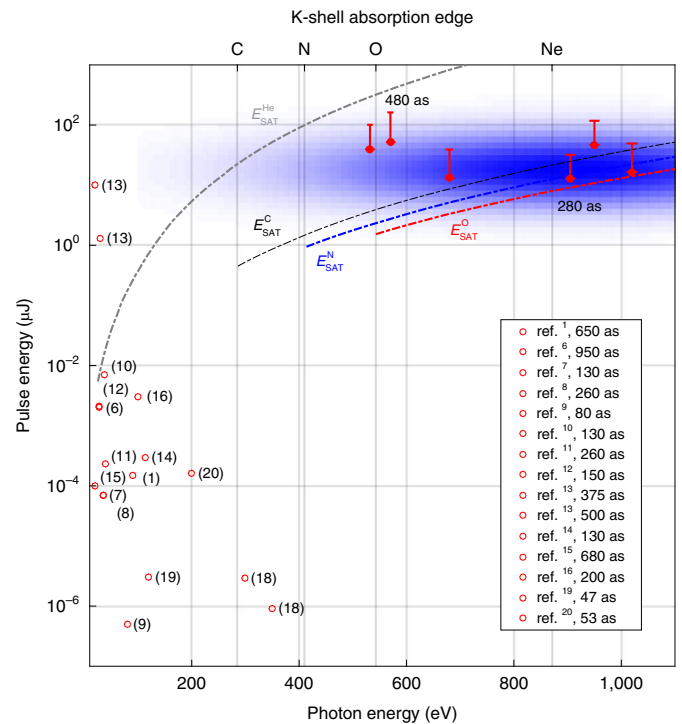


Fig. 4 | Comparison to state-of-the-art attosecond sources. Survey of published isolated attosecond pulse sources^{1,6–16,18–20} extending into the soft X-ray domain (red open circles), along with the results demonstrated in this work for a number of different photon energies (red filled circles). The filled circles show the average pulse energy recorded during the experiment, the error bar extends from the central energy and includes up to 90% of the recorded pulse energies. For the two datasets shown in Fig. 2, the measured average pulse durations are reported next to the corresponding data points. All previous results were obtained via strong-field-driven HHG with near-infrared and mid-infrared laser fields, whilst our results are obtained using an XFEL source. As a first-order estimate of the propensity for nonlinear spectroscopy (pump–probe spectroscopy, for example) we show the pulse energy required to saturate 1s ionization of carbon (dash-dot, black), nitrogen (dash-dot, blue), oxygen (dash-dot, red) and helium (dash-dot, grey), assuming a $1 \mu\text{m}^2$ focal spot size, as a function of X-ray photon energy. Sources within two orders of magnitude of these lines are likely sources for pump–probe studies. The legend in the bottom right corner gives the published pulse duration for the previous measurements. The shaded blue area shows the operational range predicted for LCLS-II.

The median FWHM bandwidth is 7.5 eV and 5 eV for the 905 eV and 650 eV datasets respectively. The statistical distribution of pulse energies in Fig. 3e shows a better relative stability than in Fig. 3f largely due to more stable electron beam conditions. The Fourier transform limited (FTL) duration for a bandwidth of 7.5 eV (5 eV) is 240 as (365 as). The average pulse duration recovered from our reconstruction at similar energies is within a factor of two of the FTL value. This discrepancy is due to the beam energy chirp introduced by longitudinal space-charge forces within the high-current ESASE spike⁵³ and the corresponding undulator taper required for sustained resonant interaction between X-rays and electrons (see Supplementary Information). From the undulator taper, we infer a residual chirp in the emitted X-rays of roughly $+12 \text{ eV fs}^{-1}$ ($+5 \text{ eV fs}^{-1}$) for the 920 eV (605 eV) data. The positive sign indicates that the higher-energy photons arrive first. This is consistent with the measured time–bandwidth product. Ripples in the spectral intensity are visible in the 650 eV spectra and are due to interference with satellite pulses. The pulse energies of these side pulses can

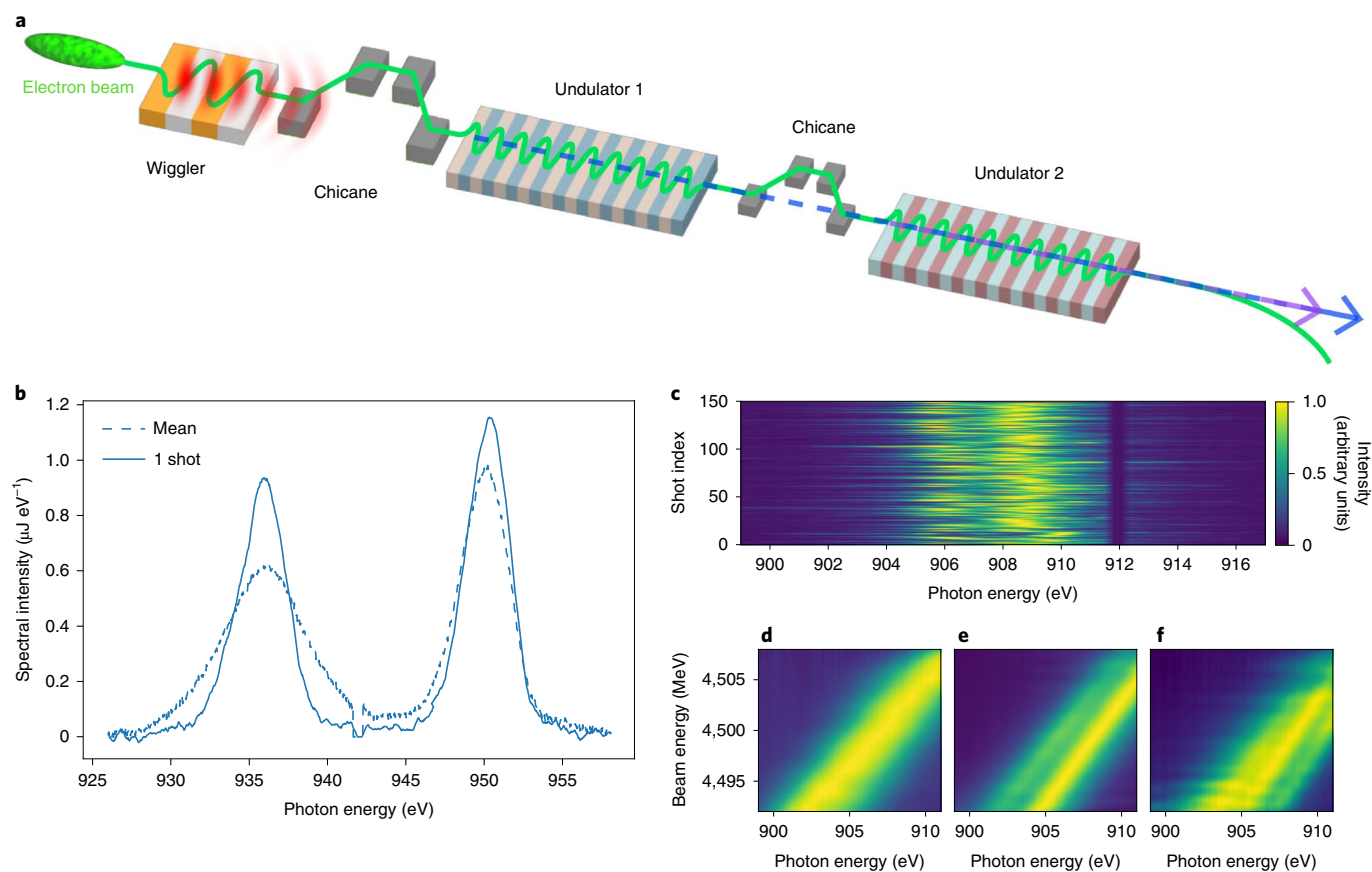


Fig. 5 | Double-pulse measurements. **a**, Schematic representation of the double-pulse-generation experiment. The electron beam is modulated and compressed in the XLEAP beamline and sent to the LCLS undulator. The undulator is divided into two parts separated by a magnetic chicane. Each half of the undulator is used to generate an X-ray pulse with different pulse energies, and the chicane introduces a variable delay between the pulses. **b**, Single-shot and average two-colour spectra measured with a grating spectrometer. **c**, Single-shot measurements of the spectrum of the pulse pair of the same photon energy with 1 fs delay. The repeatable spectral fringes demonstrate phase stability between the pulses. **d–f**, Averaged phase-stable double-pulse spectra as a function of photon energy and electron beam energy for a nominal chicane delay of 0 fs (single pulse) (**d**), 0.5 fs (**e**) and 3 fs (**f**) (same colour scale as in **c**).

be inferred from the single-shot spectra and are typically less than 0.3% of the main pulse for 650 eV and negligible for 905 eV.

Considerations for pump–probe spectroscopy

To put the results of our work in context, we detail the development of isolated attosecond pulse sources in Fig. 4, where we compare the measured pulse energy from existing attosecond light sources with the requisite flux to saturate the ionization of 1s electrons in various atomic systems. The saturation level serves as a coarse approximation to the energy required for a pump–probe experiment, and sources within two orders of magnitude of saturation are likely to be useful for pump–probe studies. The pulse energy produced by HHG sources decays very rapidly with the photon energy and is several orders of magnitude below the threshold for nonlinear interaction in the soft X-ray range ($E > 280$ eV). Conversely, our method can produce isolated attosecond pulses with tens of microjoules of pulse energy, increasing the available pulse energy at soft X-ray wavelengths by six orders of magnitude, and reaching intensities sufficient for attosecond pump–attosecond probe experiments. Note that Fig. 4 reports the pulse energy measured for the experiments shown in Figs. 2 and 3, as well as other experiments using the XLEAP set-up at different photon energies. The highest observed median pulse energy is ~ 50 μJ .

In addition to high single-pulse photon flux, the application of this technique to attosecond pump–attosecond probe experiments requires the generation of pairs of synchronized pulses. Ideally,

these pulses could have different photon energies, allowing for excitation at one atomic site in a molecular system to be probed at another⁵⁴. To this end, ESASE can be easily adapted to generate pairs of pulses of different colours using the split undulator method⁵⁵. In this scheme, the LCLS undulator is divided into two parts separated by a magnetic chicane, as shown in Fig. 5a. The ESASE current spike is used to generate two X-ray pulses of different energies in the two undulators. The magnetic chicane delays the electrons with respect to the X-rays, thus introducing a controllable delay between the first and second X-ray pulses.

Figure 5 shows the results of such a double-pulse ESASE experiment at the LCLS. Two pulses with an average pulse energy of 6 μJ each and an energy separation of 15 eV were generated (Fig. 5b). The timing jitter between the two pulses was not measured, but numerical simulations indicate that it is shorter than the individual pulse duration (see for example ref. 52). We note that the energy separation range in our experiment is limited by the tuning range of the LCLS undulator (roughly 3% of the photon energy⁵⁵), but this scheme could be used with variable-gap undulators and allow fully independent tuning of the two colours. This will be possible with the upcoming LCLS-II upgrade, enabling continuous tuning between 250 eV and 1,200 eV (ref. 56). The temporal separation can be varied from a minimum of 2 fs up to a maximum of roughly 50 fs. Smaller delays could be accessed with a gain-modulation scheme⁵⁷. Improved two-colour operation with higher peak power and delay control through overlap will be achieved with the planned upgrade of the XLEAP set-up⁵².

Using the split-undulator scheme shown in Fig. 5a, one can also generate two pulses of the same photon energy and with mutual phase stability. Unlike the case of two different colours, where the two pulses are seeded by noise at different frequencies and are uncorrelated, in this case the beam microbunching that generates the first pulse is re-used to generate a second pulse, and the two are phase-locked. Figure 5c–f shows the measured spectra under these conditions. The spectra exhibit stable and repeatable fringes, which implies that the phase between the two pulses is stable to better than the X-ray wavelength. From the variation in the spectral fringes we can infer a phase jitter of 0.77 rad, or 0.5 as between the pulses. In this case the delay can be varied from 0 fs to roughly 5 fs, beyond this value, the delay chicane will destroy the X-ray microbunching and hence the phase stability of the pulses. This level of interferometric stability could also be achieved for two different colours by exploiting harmonic microbunching generated in the first undulator³⁷, and tuning the second undulator to a harmonic of the first pulse.

Summary and conclusions

We have demonstrated a source of tunable sub-femtosecond X-ray pulses with unprecedented peak power using an XFEL. The pulses were generated by an electron bunch modulated by interaction with a high-power infrared light pulse and compressed in a small magnetic chicane. To diagnose the temporal structure of these pulses we used an attosecond streak camera and measured a median pulse duration of 280 as (480 as) at 905 eV (570 eV). With an eye towards pump–probe experiments, pairs of sub-femtosecond pulses were demonstrated using a split-undulator technique, showing control of the delay and energy separation. We have also shown that for short delays, two pulses of the same colour can be controlled with interferometric stability, a result that could be extended to two-colour operation by exploiting harmonic microbunching.

These pulses have photon flux millions of times greater than what can be achieved with any existing attosecond soft X-ray source. Such a marked increase in pulse energy will enable a suite of nonlinear X-ray spectroscopies, such as attosecond pump–attosecond probe experiments^{26,58} and four-wave mixing protocols⁵⁴, that would be impossible with any other existing technology. Moreover, the achieved photon flux will enable single-shot X-ray imaging at the attosecond timescale. Since the scheme developed in this work is based solely on a passive modulator, our technique is easily scalable to MHz repetition rates, which are envisioned for the next generation of XFELs^{34,56}. Whilst HHG-based sources have driven the attosecond revolution over the past two decades, MHz-repetition-rate XFELs, combined with the results presented here, pave the way for a new era of attosecond science.

Online content

Any methods, additional references, Nature Research reporting summaries, source data, extended data, supplementary information, acknowledgements, peer review information; details of author contributions and competing interests; and statements of data and code availability are available at <https://doi.org/10.1038/s41566-019-0549-5>.

Received: 7 July 2019; Accepted: 14 October 2019;

Published online: 02 December 2019

References

- Hentschel, M. et al. Attosecond metrology. *Nature* **414**, 509–513 (2001).
- Li, X. F. et al. Multiple-harmonic generation in rare gases at high laser intensity. *Phys. Rev. A* **39**, 5751–5761 (1989).
- Corkum, P. B. & Krausz, F. Attosecond science. *Nat. Phys.* **3**, 381–387 (2007).
- Chang, Z. & Corkum, P. Attosecond photon sources: the first decade and beyond [invited]. *J. Opt. Soc. Am. B* **27**, B9–B17 (2010).
- Ciappina, M. F. et al. Attosecond physics at the nanoscale. *Rep. Prog. Phys.* **80**, 054401 (2017).
- Sekikawa, T., Kosuge, A., Kanai, T. & Watanabe, S. Nonlinear optics in the extreme ultraviolet. *Nature* **432**, 605–608 (2004).
- Sansone, G. et al. Isolated single-cycle attosecond pulses. *Science* **314**, 443–446 (2006).
- Sola, I. J. et al. Controlling attosecond electron dynamics by phase-stabilized polarization gating. *Nat. Phys.* **2**, 319–322 (2006).
- Goulielmakis, E. et al. Single-cycle nonlinear optics. *Science* **320**, 1614–1617 (2008).
- Mashiko, H. et al. Double optical gating of high-order harmonic generation with carrier-envelope phase stabilized lasers. *Phys. Rev. Lett.* **100**, 103906 (2008).
- Feng, X. et al. Generation of isolated attosecond pulses with 20 to 28 femtosecond lasers. *Phys. Rev. Lett.* **103**, 183901 (2009).
- Ferrari, F. et al. High-energy isolated attosecond pulses generated by above-saturation few-cycle fields. *Nat. Photon.* **4**, 875–879 (2010).
- Takahashi, E. J., Lan, P., Mcke, O. D., Nabekawa, Y. & Midorikawa, K. Attosecond nonlinear optics using gigawatt-scale isolated attosecond pulses. *Nat. Commun.* **4**, 2691 (2013).
- Ossiander, M. et al. Attosecond correlation dynamics. *Nat. Phys.* **13**, 280–285 (2017).
- Barillot, T. R. et al. Towards XUV pump-probe experiments in the femtosecond to sub-femtosecond regime: new measurement of the helium two-photon ionization cross-section. *Chem. Phys. Lett.* **683**, 38–42 (2017).
- Bergues, B. et al. Tabletop nonlinear optics in the 100-eV spectral region. *Optica* **5**, 237–242 (2018).
- Jahn, O. et al. Towards intense isolated attosecond pulses from relativistic surface high harmonics. *Optica* **6**, 280–287 (2019).
- Teichmann, S. M., Silva, F., Cousin, S. L., Hemmer, M. & Biegert, J. 0.5-keV soft X-ray attosecond continua. *Nat. Commun.* **7**, 11493 (2016).
- Gaumnitz, T. et al. Streaking of 43-attosecond soft-X-ray pulses generated by a passively CEP-stable mid-infrared driver. *Opt. Express* **25**, 27506–27518 (2017).
- Li, J. et al. 53-attosecond X-ray pulses reach the carbon K-edge. *Nat. Commun.* **8**, 186 (2017).
- Johnson, A. S. et al. High-flux soft x-ray harmonic generation from ionization-shaped few-cycle laser pulses. *Sci. Adv.* **4**, eaar3761 (2018).
- Wolf, T. J. A. et al. Probing ultrafast $\pi\pi^*/\pi\pi^*$ internal conversion in organic chromophores via K-edge resonant absorption. *Nat. Commun.* **8**, 29 (2017).
- Neville, S. P., Chergui, M., Stollow, A. & Schuurman, M. S. Ultrafast X-ray spectroscopy of conical intersections. *Phys. Rev. Lett.* **120**, 243001 (2018).
- Attar, A. R. et al. Femtosecond x-ray spectroscopy of an electrocyclic ring-opening reaction. *Science* **356**, 54–59 (2017).
- Schütte, B. et al. Bright attosecond soft X-ray pulse trains by transient phase-matching in two-color high-order harmonic generation. *Opt. Express* **23**, 33947–33955 (2015).
- Leone, S. R. et al. What will it take to observe processes in 'real time'? *Nat. Photon.* **8**, 162–166 (2014).
- Lépine, F., Ivanov, M. Y. & Vrakking, M. J. J. Attosecond molecular dynamics: fact or fiction? *Nat. Photon.* **8**, 195–204 (2014).
- Ackermann, W. et al. Operation of a free-electron laser from the extreme ultraviolet to the water window. *Nat. Photon.* **1**, 336–342 (2007).
- Emma, P. et al. First lasing and operation of an ångström-wavelength free-electron laser. *Nat. Photon.* **4**, 641–647 (2010).
- Allaria, E. et al. Highly coherent and stable pulses from the FERMI seeded free-electron laser in the extreme ultraviolet. *Nat. Photon.* **6**, 699–704 (2012).
- Allaria, E. et al. Two-stage seeded soft-X-ray free-electron laser. *Nat. Photon.* **7**, 913–918 (2013).
- Ishikawa, T. et al. A compact X-ray free-electron laser emitting in the sub-ångström region. *Nat. Photon.* **6**, 540–544 (2012).
- Kang, H.-S. et al. Hard X-ray free-electron laser with femtosecond-scale timing jitter. *Nat. Photon.* **11**, 708–713 (2017).
- Altarelli, M. The European X-ray free-electron laser facility in Hamburg. *Nuclear Instrum. Methods Phys. Res. Sect. B* **269**, 2845–2849 (2011).
- Bonifacio, R., Pellegrini, C. & Narducci, L. Collective instabilities and high-gain regime in a free-electron laser. *Opt. Commun.* **50**, 373–378 (1984).
- Pellegrini, C., Marinelli, A. & Reiche, S. The physics of x-ray free-electron lasers. *Rev. Mod. Phys.* **88**, 015006 (2016).
- Huang, Z. & Kim, K.-J. Review of x-ray free-electron laser theory. *Phys. Rev. ST Accel. Beams* **10**, 034801 (2007).
- Bonifacio, R., DeSalvo, L., Pierini, P., Piovella, N. & Pellegrini, C. Spectrum, temporal structure, and fluctuations in a high-gain free-electron laser starting from noise. *Phys. Rev. Lett.* **73**, 70–73 (1994).
- Huang, S. et al. Generating single-spike hard x-ray pulses with nonlinear bunch compression in free-electron lasers. *Phys. Rev. Lett.* **119**, 154801 (2017).
- Marinelli, A. et al. Experimental demonstration of a single-spike hard-X-ray free-electron laser starting from noise. *Appl. Phys. Lett.* **111**, 151101 (2017).
- Behrens, C. et al. Few-femtosecond time-resolved measurements of X-ray free-electron lasers. *Nat. Commun.* **5**, 3762 (2014).
- Hartmann, N. et al. Attosecond time-energy structure of X-ray free-electron laser pulses. *Nat. Photon.* **12**, 215–220 (2018).

43. Zholents, A. A. Method of an enhanced self-amplified spontaneous emission for x-ray free electron lasers. *Phys. Rev. ST Accel. Beams* **8**, 040701 (2005).
44. MacArthur, J. P. et al. Phase-stable self-modulation of an electron beam in a magnetic wiggler. *Phys. Rev. Lett.* **123**, 214801 (2019).
45. Li, S. et al. A co-axial velocity map imaging spectrometer for electrons. *AIP Adv.* **8**, 115308 (2018).
46. Kienberger, R. et al. Atomic transient recorder. *Nature* **427**, 817–821 (2004).
47. Kazansky, A. K., Bozhevolnov, A. V., Sazhina, I. P. & Kabachnik, N. M. Interference effects in angular streaking with a rotating terahertz field. *Phys. Rev. A* **93**, 013407 (2016).
48. Kazansky, A. K., Sazhina, I. P., Nosik, V. L. & Kabachnik, N. M. Angular streaking and sideband formation in rotating terahertz and far-infrared fields. *J. Phys. B* **50**, 105601 (2017).
49. Li, S. et al. Characterizing isolated attosecond pulses with angular streaking. *Opt. Express* **26**, 4531–4547 (2018).
50. Itatani, J. et al. Attosecond streak camera. *Phys. Rev. Lett.* **88**, 173903 (2002).
51. Glowina, J. M. et al. Time-resolved pump-probe experiments at the LCLS. *Opt. Express* **18**, 17620–17630 (2010).
52. Zhang, Z., Duris, J., MacArthur, J. P., Huang, Z. & Marinelli, A. Double chirp-taper x-ray free-electron laser for attosecond pump-probe experiments. *Phys. Rev. Accel. Beams* **22**, 050701 (2019).
53. Ding, Y., Huang, Z., Ratner, D., Bucksbaum, P. & Merdji, H. Generation of attosecond x-ray pulses with a multicycle two-color enhanced self-amplified spontaneous emission scheme. *Phys. Rev. ST Accel. Beams* **12**, 060703 (2009).
54. Mukamel, S., Healion, D., Zhang, Y. & Biggs, J. D. Multidimensional attosecond resonant X-ray spectroscopy of molecules: lessons from the optical regime. *Annu. Rev. Phys. Chem.* **64**, 101–127 (2013).
55. Lutman, A. A. et al. Experimental demonstration of femtosecond two-color x-ray free-electron lasers. *Phys. Rev. Lett.* **110**, 134801 (2013).
56. Schoenlein, R. et al. *New Science Opportunities Enabled by LCLS-II X-ray Lasers* SLAC Pub. SLAC-R-1053 https://portal.slac.stanford.edu/sites/lcls_public/Documents/LCLS-II_ScienceOpportunities_final.pdf (SLAC National Accelerator Laboratory, 2015).
57. Marinelli, A. et al. Multicolor operation and spectral control in a gain-modulated X-ray free-electron laser. *Phys. Rev. Lett.* **111**, 134801 (2013).
58. Schweigert, I. V. & Mukamel, S. Probing valence electronic wave-packet dynamics by all X-ray stimulated Raman spectroscopy: a simulation study. *Phys. Rev. A* **76**, 012504 (2007).

Publisher's note Springer Nature remains neutral with regard to jurisdictional claims in published maps and institutional affiliations.

© The Author(s), under exclusive licence to Springer Nature Limited 2019

Methods

XFEL set-up. The XFEL at the LCLS is composed of a high-brightness linear accelerator (linac) and a magnetic undulator. The XLEAP beamline is composed of a long-period wiggler and a magnetic chicane before the undulator section. The accelerator and undulator/wiggler parameters used in this experiment are summarized in the Supplementary Information. X-rays generated in the undulators are focused with a pair of Kirkpatrick–Baez mirrors to a spot size of ~ 55 μm diameter (FWHM). More information on the XFEL parameters is given in the Supplementary Information.

Streaking laser set-up. The streaking laser pulse is derived from a 120 Hz titanium-doped sapphire laser system synchronized to the accelerator. 10 mJ, 800 nm laser pulses are compressed to ~ 40 fs, and the compressed pulse is used to pump an optical parametric amplifier (TOPAS-HE, Light Conversion) that produces 500 μJ pulses at a wavelength of 1,300 nm. The 1,300 nm pulse is spectrally filtered to remove any residual pump light or any other colours made by the optical parametric amplifier. A quarter-wave plate (Thorlabs AQWP05M-1600) is used to produce circularly polarized laser pulses, which are then focused with a 750 mm focal length CaF_2 lens. A dichroic mirror (R1300/T400-550) is used to steer the beam into a vacuum chamber. The streaking laser field is combined with the XFEL beam using a silver mirror with a 2-mm-diameter drilled hole, and both pulses come to a common focus in the interaction region of a coaxial velocity map imaging apparatus⁴⁵. The laser is focused to a diameter of ~ 110 μm . More information on the laser configuration along with additional figures showing the experimental geometry are available in the Supplementary Information.

Photoelectron spectrometer. Our experiment was performed at the Atomic, Molecular, and Optical physics (AMO) beamline of the LCLS. Photoelectrons produced by two-colour ionization are collected in our coaxial velocity map imaging apparatus⁴⁵. Photoelectrons are extracted in the direction opposite to the laser propagation direction, as shown in the Supplementary Information. Extracted electrons are detected with a microchannel plate detector coupled to a P43 phosphor screen. The phosphor screen is imaged onto a high-speed charge-coupled device (CCD) camera (Opal1k) via the 2 mm holey mirror that couples the streaking laser into the chamber, and through the dichroic mirror. The CCD camera records images of the phosphor screen at the repetition rate of the accelerator, 120 Hz. A target gas is introduced via a molecular beam source, which crosses with the XFEL and streaking laser beams in the interaction region. For the two X-ray photon energies considered in the main text, we use neon as the target for the 905 eV pulses and CO_2 as the target for the 570 eV pulses. More information on the experimental set-up and analysis of the measured photoelectron momentum distribution is given in the Supplementary Information.

Data availability

A subset of the raw data used to produce Figs. 2–5 is publicly available at figshare (https://figshare.com/projects/Tunable_Isolated_Attosecond_X-ray_Pulses_with_Gigawatt_Peak_Power_from_a_Free-Electron_Laser/65741). This repository also contains a copy of the analysis script used to invert the photoelectron momentum distributions. All other data that support the plots within this paper and other findings of this study are available from the corresponding authors on reasonable request.

Acknowledgements

We would like to acknowledge T. Gorkhover, C. Bostedt, C. Pellegrini, A. Cavalieri, N. Berrah, L. Young, L. F. DiMauro, H.-D. Nuhn, G. Marcus, T. Maxwell, M. Dunne, M. Minitti and R. Schoenlein for useful discussions and suggestions. We would also like to acknowledge M. Merritt, O. Schmidt, N. Strelnikov and I. Vasserman for their assistance in designing, constructing and installing the XLEAP wiggler. We also acknowledge the SLAC Accelerator Operations and the LCLS operations group, and the Mechanical and Electrical engineering divisions of the SLAC Accelerator Directorate, especially G. Kraft, M. Carrasco, A. Cedillos, K. Luchini, D. Bohler and J. Mock for their invaluable support. This work was supported by US Department of Energy contract nos. DE-AC02-76SF00515, DOE-BES Accelerator and detector research program Field Work Proposal 100317, DOE-BES, Chemical Sciences, Geosciences, and Biosciences Division, and Department of Energy, Laboratory Directed Research and Development program at SLAC National Accelerator Laboratory, under contract DE-AC02-76SF00515. W.H. acknowledges financial support by the BACATEC programme. P.R. and M.F.K. acknowledge additional support by the DFG via KL-1439/10, and the Max Planck Society. G.H. acknowledges the Deutsche Forschungsgemeinschaft (DFG, German Research Foundation) Projektnummer 328961117 SFB 1319 ELCH. A.Z. and J.Z.X. acknowledge support by the US Department of Energy contract no. DE-AC02-06CH11357. J.P.Marangos and T.D. acknowledge support by EPSRC programme grant EP/R019509/1.

Author contributions

A.M. and J.P.C. conceived the experiment, led the experimental team and data analysis and co-wrote the article. J.D. led the electron bunch shaping experimental work and spectral measurement, analysed the spectral data and co-wrote the paper. S.L. designed and built the streaking instrument, participated in the streaking experiment, performed the streaking data analysis and co-wrote the article. T.D. and E.G.C. participated in the streaking experiment, contributed to the streaking data analysis and co-wrote the article. J.P.MacArthur, A.A.L. and Z.Z. participated in the streaking experiment and the electron bunch experimental development, and co-wrote the article. P.R., J.W.A., G.C., J.M.G., G.H., A.K., J.Knurr, J.Krzywinski, M.-F.L., M.N., J.T.O'N., N.S., P.W., A.L.W., T.J.A.W. and M.F.K. participated in the streaking experiment and co-wrote the article. J.Z.X. designed the magnetic wiggler and oversaw the construction of the magnetic wiggler and co-wrote the article. F.-J.D. contributed to the electron bunch shaping development and co-wrote the article. A.Z. helped conceive the experiment and contributed to the design of the magnetic wiggler and co-wrote the article. J.J.W. helped conceive and design the XLEAP beamline and co-wrote the article. Z.H. helped conceive the experiment and design the XLEAP beamline, participated in the electron bunch shaping experiments and co-wrote the article. P.H.B., W.H., A.N. and R.C. helped conceive and participated in the streaking experiment and co-wrote the article. J.P.Marangos helped conceive the experiment and co-wrote the article.

Competing interests

The authors declare no competing interests.

Additional information

Supplementary information is available for this paper at <https://doi.org/10.1038/s41566-019-0549-5>.

Correspondence and requests for materials should be addressed to J.P.C. or A.M.

Reprints and permissions information is available at www.nature.com/reprints.